The Influence of Silicateins on the Shape and Crystalline Habit of Silica Carbonate Biomorphs of Alkaline Earth Metals (Ca, Ba, Sr)

Nuria Sánchez-Puig [1,*], Mayra Cuéllar-Cruz [2], Selene R. Islas [3], Juana V. Tapia-Vieyra [1], Roberto A. Arreguín-Espinosa [1] and Abel Moreno [1,*]

[1] Instituto de Química, Universidad Nacional Autónoma de México, Avenida Universidad 3000, Ciudad Universitaria, Ciudad de México 04510, Mexico; jvtvieyra@hotmail.com (J.V.T.-V.); arrespin@unam.mx (R.A.A.-E.)

[2] Departamento de Biología, División de Ciencias Naturales y Exactas, Campus Guanajuato, Universidad de Guanajuato, Noria Alta S/N, Col. Noria Alta, Guanajuato 36050, Mexico; mcuellar@ugto.mx

[3] Instituto de Ciencias Aplicadas y Tecnología, Universidad Nacional Autónoma de México, Circuito Exterior S/N, Ciudad Universitaria, Ciudad de México 04510, Mexico; selene.islas@icat.unam.mx

* Correspondence: nuriasp@unam.mx (N.S.-P.); carcamo@unam.mx (A.M.)

Abstract: This contribution presents the effect of two ortholog enzymes from marine sponges called silicateins on the formation of silica carbonate biomorphs of alkaline metals (Ca, Ba, Sr). In vivo, these enzymes participate in the polymerization of silica. Silicateins from *Tethya aurantia* and *Suberitis domuncula* were produced recombinantly and presented different degrees of activity, as evidenced by their ability to cleave silyl ether-like bonds in a model compound. Biomorphs are typically inorganic structures that show characteristic shapes resembling those of biological structures such as helices, leaves, flowers, disks or spheres. Irrespective of the concentration or the enzyme used, the presence of silicateins inhibited the formation of classic morphologies of biomorphs, albeit to different extents. Thus, not only the silica condensation activity of the enzyme but also its ability to bind silica compounds is implicated in the inhibition process. The largest effect was observed for the strontium and barium biomorphs, leading to the formation of spheres similar to those observed in diatoms and Radiolaria rather than the classical non-symmetrical forms. Characterization of the samples using Raman spectroscopy showed that silicatein did not affect the crystalline structure of the alkaline earth metal carbonate but did modify the crystalline habit.

Keywords: biomorphs; silicateins; silica carbonate biomorphs; *Tethya aurantia*; *Suberitis domuncula*

1. Introduction

Humans have always been fascinated by the variety of natural shapes and forms adopted in life. The perfect and regular shapes of gems, such as diamonds, rubies and sapphires, or minerals, such as quartz, galena and calcite, among others, have made them highly valuable in our society. Exquisite architectures are also found in biological structures resulting from the interplay between inorganic material and organic molecules, such as those found in diatoms and marine sponge skeletons or abalone shells [1]. Everything in nature has a curvature, a hallmark of most living organisms, and understanding the underlying physical phenomena that produce such stunning structures has not been as simple as appreciating them. Here, we studied a type of fascinating complex microstructure called biomorphs, which are formed by the co-precipitation of alkaline earth metal carbonates and amorphous silica in alkaline conditions. Biomorphs were discovered at the beginning of the twentieth century and display a variety of life-like shapes [2,3], such as cardioid leaves, helical filaments, wavy sheets and conical funnels [4–6]. These biomorphs are synthesized by neutralizing sodium metasilicate with an acidic solution containing carbon dioxide from the environment under the presence of alkaline earth metals [7]. In the past

fifty years, several techniques have been developed for the synthesis and characterization of these biomorphs [8]. Several studies published elsewhere have evaluated the impact of physical parameters including temperature [8], electric fields [9], UV light [10], pH, CO_2 content and growth in solution or gels on the formation of biomorphs [11–14]. In addition, the influence of cationic additives [15] and biomolecules such as nucleic acids and amino acids in the synthesis of these biomorphs has also been recently reviewed [16,17]. During the synthesis of biomorphs, carbonate ions supplied either in situ or dissolved from the CO_2 in the environment react with the alkaline earth metal salt to precipitate the corresponding crystalline carbonate. The crystallites adsorb to the surface of the silica present as silicic acid, $[Si(OH)_4]$, poisoning their crystal growth and causing bifurcation of the crystal, which results in the characteristic curvy shapes observed in the biomorphs [7]. Thus, biomorphs are dual composite nanocrystals consisting of the corresponding alkaline earth metal carbonate and amorphous silica (SiO_2). In nature, marine organisms such as sponges and diatoms use proteins to make their silica skeletons by polymerizing silicic acid. Diatoms use small polypeptides called silaffins [18], while sponges mainly employ an enzyme named silicatein [19]; other organic biomolecules, such as hexosamine-containing small molecules, and proteins with large amounts of aspartic acid, glutamic acid, glycine and histidine, such as Glassin [20], have also been described.

Poriferans, commonly referred to as sponges, are among the oldest animal fossils ever recorded, dating back to the Ediacaran period (600 Ma) [21,22]. This fossil evidence is considered as the divergent point between the sponge and eumetazoan lineages and thus they have great significance in the reconstruction of early metazoan evolution. Phylogenomic analyses have shown that these two lineages, derived from a common ancestor [23], are predicted to have existed in the Cryogenian—the geological period at the end of the Snowball Earth glaciations of 635 Ma. The phylum Porifera is composed of four distinct classes: Hexactinellida, Demospongia, Calcarea and Homoscleromorpha [24]. The Hexactinellida or glass sponges are remarkably different from other sponges in many aspects of their biology. Of particular interest is their ability to form inorganic silica structures known as spicules, which constitute their skeleton. Silica is deposited in the form of opaline silica, $SiO_2 \cdot nH_2O$, together with small amounts of other minerals including sulfur, aluminum, potassium, calcium and sodium. Spicules grow in a radiate incremental manner along a central axial canal which contains an organic filament composed mainly of an enzyme named silicatein [19,25]. This enzyme is also found in the extraspicular space, where it contributes to the appositional growth of the skeletal elements, acting not only in the enzymatic polycondensation reaction of poly(silicate) but also as a template for silica deposition [26]. Silicateins are members of the proteinases cathepsin subfamily, with a similar Xaa–His–Asn catalytic triad at their active site, although silicateins have a Ser residue in the Xaa position rather than Cys as in cathepsin L. Silicateins have a large tendency to self-assemble and form organized condensed fibers of 70–100 nm. They also associate with silintaphin-1 to form oligomers which interact with each other, creating fractal intermediate structures through a diffusion-limited process [27,28]. Besides the physiological role of silicatein, in vitro, it is able to hydrolyze and condensate Si–O bonds [29] of diverse organosilanols and silyl ethers and also to catalyze transetherifications, where the silyl group from one silyl ether is transferred to a recipient alcohol [30]. Furthermore, silicateins can also act on related metal oxides such as gallium nitrate, leading to the deposition of gallium oxyhydroxide [31,32], or form nanoparticles of zirconia and titania using appropriate precursors [33]. These properties place silicateins as key tools to study organosiloxane chemistry and develop efficient and selective biocatalysts. The biological deposition of silica is a fascinating phenomenon, not only from the visual perspective of the intricate and exquisite structures present in the skeleton of glass sponges and diatoms but also by the fact that it occurs under physiological conditions at neutral pH, ambient pressure and temperatures between 5 and 37 °C.

In this study, the impact of silicateins on the synthesis of silica carbonate biomorphs using different alkaline metals (Ca, Ba, Sr) was investigated. We used two silicatein

orthologs with different degrees of activity as judged by their ability to cleave an ether-like bond from a silicon model compound. The morphology of the resulting biomorphs was assessed by scanning electron microscopy (SEM), while their chemical composition and crystalline structure were determined using micro-Raman spectroscopy. Irrespective of the presence of silicatein, silica carbonate biomorphs obtained from calcium, barium and strontium carbonate corresponded to the calcite, witherite aragonite-type and strontianite crystalline structures, respectively. The presence of silicateins inhibited the formation of classic biomorph morphologies regardless of the tested concentration or their activity, resulting in sphere-like shapes.

2. Materials and Methods

2.1. Protein Expression and Purification

Silicatein-α orthologues were recombinantly expressed in *E. coli* C41 (DE3) encoding residues 115–330 of the silicatein isoform α of *T. aurantia* and *S. domuncula*, hereby referred to as Ta_Silα and Sd_Silα, respectively. Ta_Silα was expressed and purified as described in [34]. The expression vector for Sd_Silα was a kind gift from Lu Shin Wong, Manchester Institute of Biotechnology, University of Manchester. Protein expression and purification was adapted from [30]. Briefly, the protein was expressed in LB media supplemented with 100 µg/mL ampicillin for 18 h at 16 °C after induction with 0.5 mM IPTG using the pColdTF vector (Takara Bio). The expressed protein corresponds to a construct comprising a 6xHistidine tag, the *E. coli* Trigger Factor followed by the catalytic domain of *S. domuncula* silicatein-α fused to a C-terminal strep-tag. Cells were lysed by sonication and the clarified lysate loaded onto a 1 mL Strep-Tactin column (QIAGEN) equilibrated with 50 mM phosphate buffer pH 7.4, 150 mM NaCl. Bound protein was eluted using the same buffer supplemented with 2.5 mM desthiobiotin. Fractions containing the protein were collected and dialyzed against 50 mM phosphate buffer pH 7.4, 150 mM NaCl, concentrated, stored at 4 °C and used within 3 days. Protein concentration was measured using the Bradford method.

2.2. Silicatein Activity Assay

Silicatein substrate bis(*p*-aminophenoxy)-dimethylsilane (BAPD-silane) was obtained from Alfa-Chemistry (USA). The silyl ether hydrolysis activity of recombinant silicatein-α was monitored as described in [29] following the increase in the absorbance signal at 300 nm of the *p*-aminophenol produced from the hydrolysis of BAPD-silane. Reactions were studied at 20 °C in the absorbance range of 230–450 nm using a Cary 60 UV–Vis spectrophotometer (Agilent Technologies). Reaction mixtures contained 230 µM BADP-silane in 50 mM phosphate buffer pH 8.4, 150 mM NaCl and 0.4 µg/mL silicatein, which corresponds to 11 nM and 5 nM of the recombinant *T. aurantia* and *S. domuncula* orthologs, respectively.

2.3. Biomorph Synthesis

The synthesis of silica carbonate biomorphs of calcium, barium and strontium was carried out by the gas-diffusion procedure published elsewhere [8]. The synthesis was performed using glass plates with dimensions of 5 mm length, 2.5 mm width and 1 mm thickness. The synthesis of biomorphs proceeded by immersing the glass pieces in the top cover (stopper) of a 1.5 mL Eppendorf tube used as a reservoir cell. Each reservoir contained 200 µL of reaction mixture consisting of 1000 ppm of sodium metasilicate, 20 mM of calcium, barium or strontium chloride, at a pH of 10.5 adjusted with sodium hydroxide. Chemical reagents were obtained from Sigma-Aldrich. As appropriate, different concentrations of each silicatein were used to evaluate their impact on biomorph formation. Experiments were performed in duplicate for each concentration of enzyme. All experiments were performed at 25 °C using a CO_2 incubator with 5% carbon dioxide saturation. Formation of biomorphs proceeded for 48 h. Figure 1 shows the schematic diagram of the different steps involved in the synthesis of biomorphs.
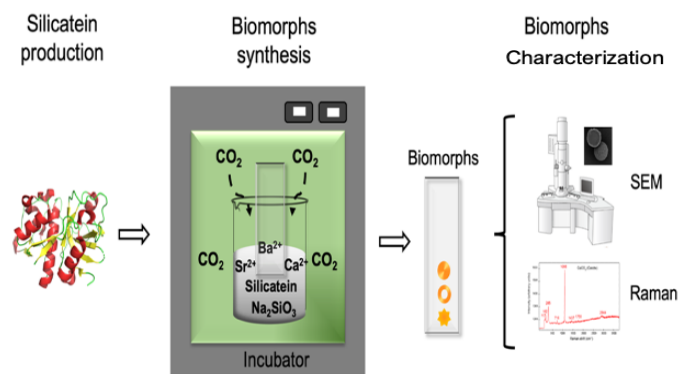
Figure 1. Schematic representation of the procedure involved in the synthesis of silica carbonate biomorphs in solution using a gas-diffusion system. The structure of the *T. aurantia* silicatein-α corresponds to that deposited in the Protein Data Bank code 6zq3.

2.4. Characterization of Biomorphs

The morphology and composition of the biomorphs were characterized according to the methodology published elsewhere [16]. Morphology of the biomorphs was assessed by scanning electron microscopy using a VEGA3 microscope (TESCAN, Brno, Czech Republic) and the crystalline habit was studied using micro-Raman spectroscopy at room temperature. Raman spectra were recorded with a WITec Alpha 300 Series Raman-AFM (WITec GmbH, Ulm, Germany) using a 672-lines/mm grating with a $100\times$ Zeiss objective (0.9 NA). The Nb:YVO4 green laser at 532 nm wavelength was used as excitation source with 14.4 mW of laser power and a spectral resolution of $1.0\ cm^{-1}$. Punctual Raman spectra were obtained with 0.5 s of integration time and 10 accumulations, and the Raman map using 0.03 s of integration time.

3. Results and Discussion

3.1. Silicatein-α Production

It is well known that the mature form of silicatein is highly hydrophobic, hampering their soluble recombinant expression [35]. Protein overexpression tends to form aggregates in the form of inclusion bodies, which are difficult to refold. Several attempts have been made to improve the solubility of these proteins, such as fusion to proteins, the use of different orthologs or varying the expression time and temperature, as well as using different host cells. In this work, we used two different silicatein orthologs that have already been expressed soluble recombinantly. The silicatein from *S. domuncula* was expressed as a fusion protein to a streptavidin tag and the Trigger Factor similarly to a previous report that used the same protein partner with a histidine tag instead [30]. On the other hand, the ortholog form *T. aurantia* was expressed as previously reported in [34], fused to residues 1–85 of the *Bacillus stearothermophilus* dihydrolipoyl acetyltransferase protein. To confirm the functionality of the two silicatein orthologs used in this study, we measured their ability to hydrolyze silyl ether bonds. Both enzymes were active, as evidenced by increasing the signal at 300 nm, resulting from the release of *p*-aminophenol after cleavage of the silyl ether-like bonds of the BADP-silane substrate (Figure 2). However, the presence of twice the amount of the *T. aurantia* silicatein resulted in the release of less product after 5 min reaction in comparison with that produced by the *S. domuncula* protein, suggesting that the former is slightly less active. This is better observed from the calculated specific activity of 16.5 nmol min^{-1} μg $protein^{-1}$ and 54 nmol min^{-1} μg $protein^{-1}$, respectively. This activity agrees well with the value of 13.5 nmol min^{-1} μg $protein^{-1}$ previously reported for the native *S. domuncula* silicatein-α using the same substrate [29]. The recombinant silicateins were used in subsequent studies to test their influence on the formation of silica carbonate biomorphs.
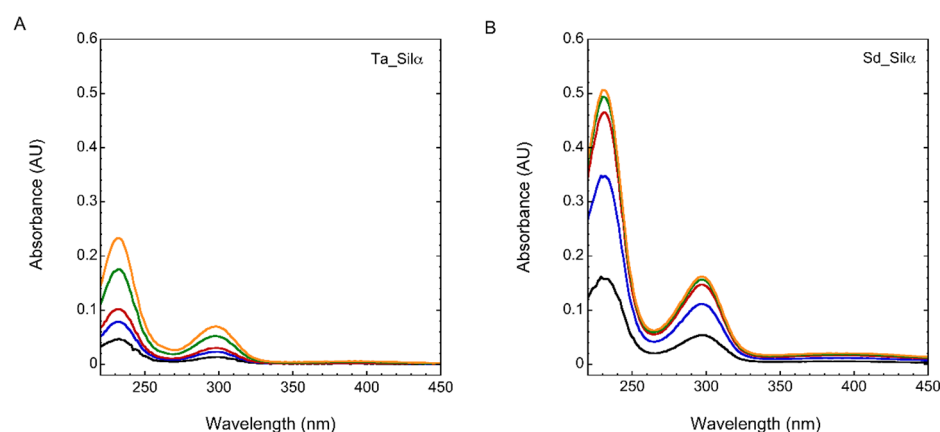
Figure 2. Silyl ether hydrolysis activity of recombinant silicatein-α from *Tethya aurantia* (**A**) and *Suberitis domuncula* (**B**). Course change in the absorption spectra upon release of *p*-aminophenol from the substrate bis(*p*-aminophenoxy)-dimethylsilane. Black—1 min, blue—2 min, red—3 min, green—4 min, yellow—5 min.

3.2. Calcium Silica Carbonate Biomorphs in the Presence of Silicatein-α

We evaluated the influence of different concentrations of silicatein-α from *T. aurantia* (Ta_silα) and *S. domuncula* (Sd_silα) in the morphology of calcium, barium and strontium silico-carbonate biomorphs by scanning electron microscopy. Figure 3 shows the effect of these enzymes when calcium was used for the synthesis of biomorphs. In the absence of enzyme, the typical rhombohedral shapes of calcium silica carbonate biomorphs were observed. In the presence of Sd_Silα at the two lower concentrations tested (10 μM and 18 μM), dendrite-like and bone-like morphologies were observed while shapes resembling flowers were obtained at the highest tested concentration. In contrast to the small effect of the *S. domuncula* silicatein, that of *T. aurantia* had a profound effect on the morphology of the biomorphs, resulting in circular druse shapes. This effect was noticeable even at lower concentrations similar to those that had no effect when tested for the Sd_Silα. At higher concentrations of Ta_Silα, sphere-like structures ranging from 4 to 10 microns were observed. This result is of particular interest as it could explain why diatoms, Radiolaria, sponges, superior plants and molluscs present different morphologies in their mineral skeletons (made either of silica or calcium carbonate). This shape control shown for the silica-carbonate biomorphs might be related to the silicatein specificity selected through evolution for each organism [19,36,37]. Similarly, calcite spherical shapes have been obtained in the presence of the intramineral proteins called struthiocalcins purified from ostrich eggshells [38].

Raman spectroscopy was used to characterize the chemical composition of the most representative calcium silico-carbonate biomorph shapes. The Raman spectra for the control calcium silico-carbonate samples consisted of rhombohedral-type structures made of calcite, as evidenced by the characteristic signal at 1089 cm^{-1} (Figure 4A). The rest of the five active modes of calcite are also present at frequencies close to theoretical values of 155, 276, 711, 1433 cm^{-1} [39]. The Raman signals for the calcium biomorphs obtained in the presence of silicatein also corresponded to those of calcite, irrespective of the enzyme tested or biomorph shape (Figure 4B,C). Although calcite is the most stable calcium carbonate polymorph and thus the most abundant in nature, commonly found in mollusc skeletons or avian eggshells [38,40], biogenic aragonite has also been described, such as that found in nacre [41]. In agreement with this, the presence of silicatein does not affect the crystalline structure of the calcium carbonate biomorphs, such that all of the evaluated ones comprise the calcite polymorph but do alter their morphologies.

3.3. Barium and Strontiun Silica Carbonate Biomorphs in the Presence of Silicatein-α

These kinds of aggregates with peculiar shapes were observed for the first time by García-Ruiz and Amorós in 1981 [42]. These structures, currently called biomorphs, are self-assembled crystalline materials that display a variety of biomimetic morphologies. These biomorphs are mainly obtained when synthesized using barium and strontium salts and consist of witherite or strontianite silica carbonate, respectively. They display the characteristic curvatures far from the restrictions of the classic crystallographic symmetry. Silica biomorphs of calcium, barium or strontium have been of great interest for several decades because their morphology and shapes are reminiscent of those found in the Precambrian cherts [11,14,42,43]. Analysis of the scanning electron microscopy images of the barium and strontium silica carbonate biomorphs depicted the classic sheets, flowers, curly- and worm-like structures (Figures 5 and 6). In contrast, incorporation of the silicateins Sd_Silα and Ta_Silα in the synthesis reaction had a remarkable effect on the resulting morphologies, which was more noticeable at higher concentrations of the enzymes (Figures 5 and 6). The shapes of the biomorphs obtained in the presence of the *S. domuncula* silicatein resembled those of the Radiolaria and diatoms of the gender *Campyloneis* [44]. The effect, however, was more pronounced for the strontium variants in the presence of the *T. aurantium* protein. Lower protein concentrations produced spherulite and sphere structures that, in some cases, grew, fusing to adjacent nucleation sites.
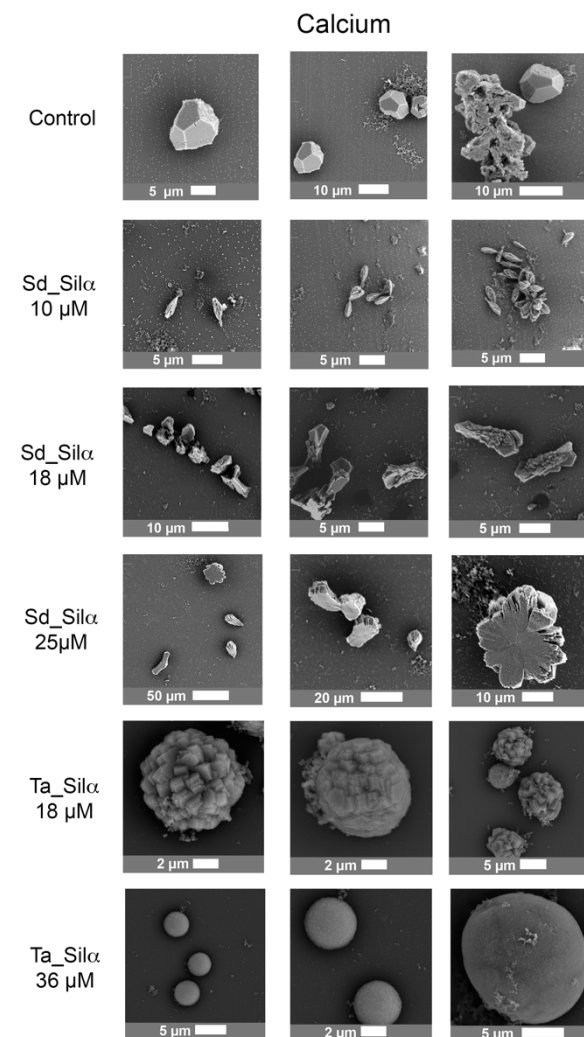
Figure 3. Selection of SEM micrographs from calcium silica carbonate biomorphs obtained at 25 °C in the presence of different concentrations of silicatein-α. Sd_Silα—*Suberitis domuncula* silicatein-α, Ta_Silα—*Tethya aurantia* silicatein-α.
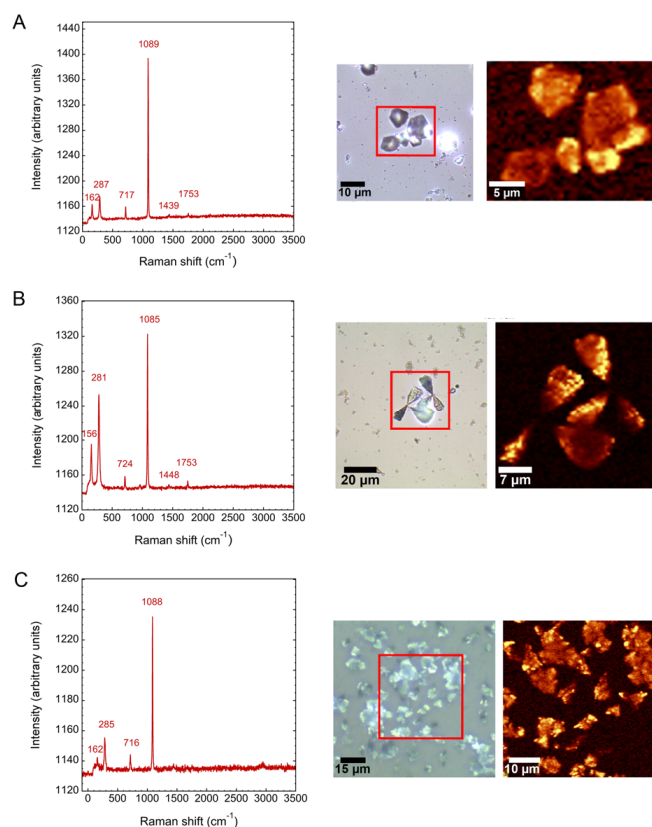
Figure 4. Raman spectroscopic analysis of calcite silica carbonate biomorphs obtained in different conditions. (**A**) Control in the absence of enzyme. (**B**) *Suberitis domuncula* silicatein-α. (**C**) *Tethya aurantia* silicatein-α. Left panels correspond to the Raman spectra. Right panels correspond to the optical image and mapping at the most intense Raman signal.

Silicateins are not found in diatoms; instead, they contain lysine- and serine-rich proteins named silaffins that participate in the biosilification process. Silaffins undergo considerable post-translational modifications, such as *O*-phosphorylation of serine residues, hydroxyprolines and hydroxylysines, making them highly hydrophilic molecules [45]. Similarly, silicateins have a unique arrangement of serine residues, rich in hydroxyl groups, that promotes the condensation of silica and polysiloxanes [19,25]. The presence of hydroxyl and charged groups is vital for the binding of silicic acid and subsequent deposition of amorphous condensed silica during biosilification. This seems an important conserved trait, not only in vivo but also in vitro, as similar spherulite biomorphs have been reported in the presence of nucleic acids which are also charged molecules [16].

Raman spectroscopy was also used to elucidate the chemical composition of the silica carbonates of barium and strontium [46]. The Raman spectra of the control barium silica carbonate (Figure 7A) show the classical frequency between 1059 and 1061 cm^{-1} corresponding to BaCO$_3$ (I), identified as the aragonite-like crystalline structure usually called witherite. Other signals close to the reported bands at 227 and 690 cm^{-1} are also present. These same signals are present in the Raman spectra of barium silica carbonate biomorphs obtained in the presence of silicateins (Figure 7B,C), suggesting that the enzymes do not modify the crystal structure. On the other hand, the Raman spectra of control strontium silica carbonate biomorphs (Figure 8A) depict an intense band at 1068 cm^{-1}, which corresponds to the signal described between 1069 and 1075 cm^{-1} and that present at 855 cm^{-1}, characteristic of the strontianite. Similar vibrations are observed in the strontium biomorphs obtained in the presence of silicateins (Figure 8B,C). In all, the presence of silicateins did not affect the crystalline structure of any of the alkaline metal carbonates but prevented the classical shape of barium and strontium silica carbonate biomorphs.

Figure 5. Selection of SEM micrographs from barium silica carbonate biomorphs obtained at 25 °C in the presence of different concentrations of silicatein-α. Sd_Silα—*Suberitis domuncula* silicatein-α, Ta_Silα—*Tethya aurantia* silicatein-α.

Figure 6. Selection of SEM micrographs from strontium silica carbonate biomorphs obtained at 25 °C in the presence of different concentrations of silicatein-α. Sd_Silα—*Suberitis domuncula* silicatein-α, Ta_Silα—*Tethya aurantia* silicatein-α.

During the synthesis of silica carbonate biomorphs under alkaline conditions, carbonate ions provided from dissolved CO_2 present in the environment react with the metal and precipitate in the corresponding salt form. The nanocrystals are then coated with a "skin" of amorphous silica, forming a composite material that prevents nuclei form growing larger. The characteristic shapes of biomorphs arise from disruption of the crystallographic symmetry arrangement of the crystal carbonate core. Transition towards a rotational symmetry produces smoothly curved surfaces, such as those resembling leaves, while a dilation route results in the fractal flower-like morphologies [7]. Because the precipitation of amorphous silica due to the formation of siloxane bonds is crucial for the formation of biomorphs, and this is coincidentally the main activity of silicateins, it was expected that their presence would aid the process and favor biomorph formation. In contrast, silicateins prevented the formation of biomorphs, irrespective of the concentration of enzyme used or the alkaline metal used. Silicatein also has the ability to direct the polymerization process in an ordered manner and, during biosilification, the protein itself ends up surrounded by silica molecules that occupy the space between the protein units in the axial filament [47]. In the scenario studied here, silicateins most likely also precipitate together with the silica in the growing front of the carbonate crystal, preventing the formation of biomorphs.
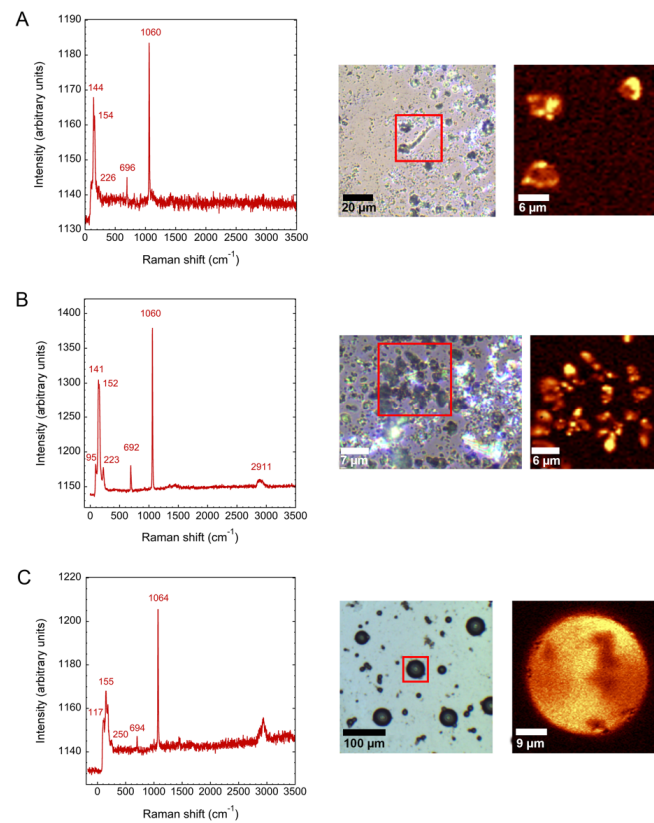
Figure 7. Raman spectroscopic analysis of witherite silica carbonate biomorphs obtained in different conditions. (**A**) Control in the absence of enzyme. (**B**) *Suberitis domuncula* silicatein-α. (**C**) *Tethya aurantia* silicatein-α. Left panels correspond to the Raman spectra. Right panels correspond to the optical image and mapping at the most intense Raman signal.
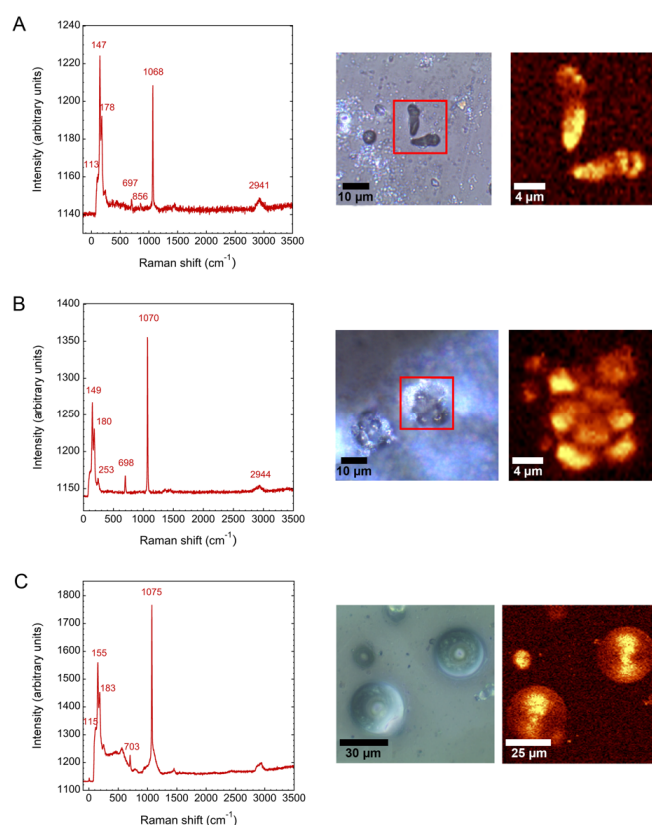
Figure 8. Raman spectroscopic analysis of strontianite silica carbonate biomorphs obtained in different conditions. (**A**) Control in the absence of enzyme. (**B**) *Suberitis domuncula* silicatein-α. (**C**) *Tethya aurantia* silicatein-α. Left panels correspond to the Raman spectra. Right panels correspond to the optical image and mapping at the most intense Raman signal.

4. Conclusions

Silicateins are multifunctional enzymes that catalyze the synthesis of biogenic silica. In this contribution, we used its ability to condensate siloxane bonds and direct the assembly of the resulting polymer to study its influence in the formation of Ca, Ba and Sr silica carbonate biomorphs. Two silicatein-α orthologs from the marine sponges *S. domuncula* and *T. aurantia* were used. The presence of any of the two enzymes affected the morphology of the biomorphs without altering their crystalline structure, which corresponded to calcite, witherite and strontianite as judged by Raman spectroscopy. The concentration of silicatein used in the assays was determinant to obtain particular shapes as it was the protein under consideration. Silicateins reshaped the classical biomorph morphologies into globular (sphere-like) structures similar to those observed in diatoms and Radiolaria. However, the precise mechanism leading to the formation of the specific forms observed and the chemical interactions happening between the silicateins and the inorganic phase of the biomorph await further investigation.

Author Contributions: Conceptualization, A.M. and N.S.-P.; methodology, M.C.-C.; S.R.I.; J.V.T.-V.; R.A.A.-E.; formal analysis, A.M.; investigation, all authors performed specific experiments; writing—original draft preparation, N.S.-P. and A.M.; writing—review and editing, A.M.; M.C.-C. and N.S.-P. All authors have read and agreed to the published version of the manuscript.

References

1. Wang, R.Z.; Addadi, L.; Weiner, S. Design strategies of sea urchin teeth: Structure, composition and micromechanical relations to function. *Philos. Trans. R. Soc. B Biol. Sci.* **1997**, *352*, 469–480. [CrossRef] [PubMed]
2. Herrera, A.L. A New Theory of the Origin and Nature of Life. *Science* **1942**, *96*, 14. [CrossRef]
3. Lillie, R.S.; Johnston, E.N. Precipitation-Structures Simulating Organic Growth. II. A Contribution to the Physico-Chemical Analysis of Growth and Heredity. *Biol. Bull.* **1919**, *36*, 225–272. [CrossRef]
4. Ruiz, J.M.G.; Kubatko, K.-A.H.; Helean, K.B.; Navrotsky, A.; Burns, P.C. Self-Assembled Silica-Carbonate Structures and Detection of Ancient Microfossils. *Science* **2003**, *302*, 1194–1197. [CrossRef] [PubMed]
5. Hyde, S.T.; Carnerup, A.M.; Larsson, A.-K.; Christy, A.G.; García-Ruiz, J.M. Self-assembly of carbonate-silica colloids: Between living and non-living form. *Phys. A: Stat. Mech. Its Appl.* **2004**, *339*, 24–33. [CrossRef]
6. Nakouzi, E.; Knoll, P.; Steinbock, O. Biomorph growth in single-phase systems: Expanding the structure spectrum and pH range. *Chem. Commun.* **2015**, *52*, 2107–2110. [CrossRef]
7. García-Ruiz, J.M.; Melero-García, E.; Hyde, S.T. Morphogenesis of Self-Assembled Nanocrystalline Materials of Barium Carbonate and Silica. *Science* **2009**, *323*, 362–365. [CrossRef]
8. Noorduin, W.L.; Grinthal, A.; Mahadevan, L.; Aizenberg, J. Rationally Designed Complex, Hierarchical Microarchitectures. *Science* **2013**, *340*, 832–837. [CrossRef]
9. Cuéllar-Cruz, M.; Moreno, A. Synthesis of Crystalline Silica-Carbonate Biomorphs of Ba(II) under the Presence of RNA and Positively and Negatively Charged ITO Electrodes: Obtainment of Graphite via Bioreduction of CO2 and Its Implications to the Chemical Origin of Life on Primitive Earth. *ACS Omega* **2020**, *5*, 5460–5469. [CrossRef]
10. Pérez, K.S.; Moreno, A. Influence of Pyruvic Acid and UV Radiation on the Morphology of Silica-carbonate Crystalline Biomorphs. *Crystals* **2019**, *9*, 67. [CrossRef]
11. García-Ruiz, J.M.; Nakouzi, E.; Kotopoulou, E.; Tamborrino, L.; Steinbock, O. Biomimetic mineral self-organization from silica-rich spring waters. *Sci. Adv.* **2017**, *3*, e1602285. [CrossRef] [PubMed]
12. Opel, J.; Kellermeier, M.; Sickinger, A.; Morales, J.; Cölfen, H.; Garcia-Ruiz, J.-M. Structural Transition of Inorganic Silica–Carbonate Composites Towards Curved Lifelike Morphologies. *Minerals* **2018**, *8*, 75. [CrossRef]
13. Opel, J.; Wimmer, F.P.; Kellermeier, M.; Cölfen, H. Functionalisation of silica–carbonate biomorphs. *Nanoscale Horiz.* **2016**, *1*, 144–149. [CrossRef]
14. Zhang, G.; Morales, J.; García-Ruiz, J.M. Growth behaviour of silica/carbonate nanocrystalline composites of calcite and aragonite. *J. Mater. Chem. B* **2017**, *5*, 1658–1663. [CrossRef]
15. Kellermeier, M.; Glaab, F.; Carnerup, A.M.; Drechsler, M.; Gossler, B.; Hyde, S.T.; Kunz, W. Additive-induced morphological tuning of self-assembled silica–barium carbonate crystal aggregates. *J. Cryst. Growth* **2009**, *311*, 2530–2541. [CrossRef]
16. Cuéllar-Cruz, M.; Islas, S.R.; Gonzalez, G.; Moreno, A. Influence of Nucleic Acids on the Synthesis of Crystalline Ca(II), Ba(II), and Sr(II) Silica–Carbonate Biomorphs: Implications for the Chemical Origin of Life on Primitive Earth. *Cryst. Growth Des.* **2019**, *19*, 4667–4682. [CrossRef]
17. Elejalde-Cadena, N.R.; Cuéllar-Cruz, M.; Moreno, A. The role of silica and alkaline earth metals with biomolecules in the biomineralization processes: The eggshell's formation and the crystallization in vivo for x-ray crystallography. *Prog. Cryst. Growth Charact. Mater.* **2020**, *66*, 100473. [CrossRef]
18. Kröger, N.; Deutzmann, R.; Sumper, M. Polycationic Peptides from Diatom Biosilica That Direct Silica Nanosphere Formation. *Science* **1999**, *286*, 1129–1132. [CrossRef]
19. Shimizu, K.; Cha, J.; Stucky, G.D.; Morse, D.E. Silicatein: Cathepsin L-like protein in sponge biosilica. *Proc. Natl. Acad. Sci. USA* **1998**, *95*, 6234–6238. [CrossRef]
20. Shimizu, K.; Amano, T.; Bari, R.; Weaver, J.C.; Arima, J.; Mori, N. Glassin, a histidine-rich protein from the siliceous skeletal system of the marine sponge Euplectella, directs silica polycondensation. *Proc. Natl. Acad. Sci. USA* **2015**, *112*, 11449–11454. [CrossRef]
21. Gehling, J.G.; Rigby, J.K. Long expected sponges from the Neoproterozoic Ediacara fauna of South Australia. *J. Paleéontol.* **1996**, *70*, 185–195. [CrossRef]
22. Yin, Z.; Zhu, M.; Davidson, E.H.; Bottjer, D.J.; Zhao, F.; Tafforeau, P. Sponge grade body fossil with cellular resolution dating 60 Myr before the Cambrian. *Proc. Natl. Acad. Sci. USA* **2015**, *112*, E1453–E1460. [CrossRef]
23. Nosenko, T.; Schreiber, F.; Adamska, M.; Adamski, M.; Eitel, M.; Hammel, J.; Maldonado, M.; Müller, W.E.; Nickel, M.; Schierwater, B.; et al. Deep metazoan phylogeny: When different genes tell different stories. *Mol. Phylogenet. Evol.* **2013**, *67*, 223–233. [CrossRef]
24. Van Soest, R.W.M.; Boury-Esnault, N.; Hooper, J.N.A.; Rützler, K.; de Voogd, N.J.; Alvarez, B.; Hajdu, E.; Pisera, A.B.; Manconi, R.; Schönberg, C.; et al. World Porifera Database. Available online: http://www.marinespecies.org/porifera (accessed on 14 April 2021).

25. Cha, J.N.; Shimizu, K.; Zhou, Y.; Christiansen, S.C.; Chmelka, B.F.; Stucky, G.D.; Morse, D.E. Silicatein filaments and subunits from a marine sponge direct the polymerization of silica and silicones in vitro. *Proc. Natl. Acad. Sci. USA* **1999**, *96*, 361–365. [CrossRef]
26. Müller, W.E.G.; Rothenberger, M.; Boreiko, A.; Tremel, W.; Reiber, A.; Schröder, H.C. Formation of siliceous spicules in the marine demosponge Suberites domuncula. *Cell Tissue Res.* **2005**, *321*, 285–297. [CrossRef]
27. Murr, M.M.; Morse, D.E. Fractal intermediates in the self-assembly of silicatein filaments. *Proc. Natl. Acad. Sci. USA* **2005**, *102*, 11657–11662. [CrossRef]
28. Schloßmacher, U.; Wiens, M.; Schröder, H.C.; Jochum, K.P.; Wang, X.; Müller, W.E.G. Silintaphin-1—Interaction with silicatein during structure-guiding bio-silica formation. *FEBS J.* **2011**, *278*, 1145–1155. [CrossRef]
29. Müller, W.E.G.; Schloßmacher, U.; Wang, X.; Boreiko, A.; Brandt, D.; Wolf, S.E.; Tremel, W.; Schröder, H.C. Poly(silicate)-metabolizing silicatein in siliceous spicules and silicasomes of demosponges comprises dual enzymatic activities (silica polymerase and silica esterase). *FEBS J.* **2007**, *275*, 362–370. [CrossRef]
30. Dakhili, S.Y.T.; Caslin, S.A.; Faponle, A.S.; Quayle, P.; De Visser, S.P.; Wong, L.S. Recombinant silicateins as model biocatalysts in organosiloxane chemistry. *Proc. Natl. Acad. Sci. USA* **2017**, *114*, E5285–E5291. [CrossRef]
31. Kisailus, D.; Choi, J.H.; Weaver, J.C.; Yang, W.; Morse, D.E. Enzymatic Synthesis and Nanostructural Control of Gallium Oxide at Low Temperature. *Adv. Mater.* **2005**, *17*, 314–318. [CrossRef]
32. Kisailus, D.; Truong, Q.; Amemiya, Y.; Weaver, J.C.; Morse, D.E. Self-assembled bifunctional surface mimics an enzymatic and templating protein for the synthesis of a metal oxide semiconductor. *Proc. Natl. Acad. Sci. USA* **2006**, *103*, 5652–5657. [CrossRef] [PubMed]
33. Tahir, M.N.; Théato, P.; Müller, W.E.G.; Schröder, H.C.; Borejko, A.; Faiss, S.; Janshoff, A.; Huth, J.; Tremel, W. Formation of layered titania and zirconia catalysed by surface-bound silicatein. *Chem. Commun.* **2005**, 5533–5535. [CrossRef]
34. Sánchez-Puig, N.; Guerra-Flores, E.; López-Sánchez, F.; Juárez-Espinoza, P.A.; Ruiz-Arellano, R.; González-Muñoz, R.; Arreguin-Espinosa, R.; Moreno, A. Controlling the morphology of silica–carbonate biomorphs using proteins involved in biomineralization. *J. Mater. Sci.* **2011**, *47*, 2943–2950. [CrossRef]
35. Schröder, H.C.; Wang, X.; Manfrin, A.; Yu, S.-H.; Grebenjuk, V.A.; Korzhev, M.; Wiens, M.; Schlossmacher, U.; Müller, W.E. Acquisition of Structure-guiding and Structure-forming Properties during Maturation from the Pro-silicatein to the Silicatein Form. *J. Biol. Chem.* **2012**, *287*, 22196–22205. [CrossRef]
36. Simpson, T.L.; Volcani, B.E. *Silicon and Siliceous Structures in Biological Systems*; Springer: Berlin/Heidelberg, Germany, 1981; p. 587.
37. Voronkov, M.G.; Zelchan, G.I.; Lukevits, E.J. *Silicon and Life*; Zinatne Publishing: Vilnius, Lithuania, 1977.
38. Ruiz-Arellano, R.R.; Moreno, A. Obtainment of Spherical-Shaped Calcite Crystals Induced by Intramineral Proteins Isolated from Eggshells of Ostrich and Emu. *Cryst. Growth Des.* **2014**, *14*, 5137–5143. [CrossRef]
39. De La Pierre, M.; Carteret, C.; Maschio, L.; André, E.; Orlando, R.; Dovesi, R. The Raman spectrum of CaCO3polymorphs calcite and aragonite: A combined experimental and computational study. *J. Chem. Phys.* **2014**, *140*, 164509. [CrossRef]
40. Reyes-Grajeda, J.P.; Moreno, A.; Romero, A. Crystal Structure of Ovocleidin-17, a Major Protein of the Calcified Gallus gallus Eggshell. *J. Biol. Chem.* **2004**, *279*, 40876–40881. [CrossRef] [PubMed]
41. Zhang, G.; Li, X. Uncovering Aragonite Nanoparticle Self-assembly in Nacre—A Natural Armor. *Cryst. Growth Des.* **2012**, *12*, 4306–4310. [CrossRef]
42. García-Ruiz, J.; Amorós, J. Morphological aspects of some symmetrical crystal aggregates grown by silica gel technique. *J. Cryst. Growth* **1981**, *55*, 379–383. [CrossRef]
43. Schopf, J.W. Solution to Darwin's dilemma: Discovery of the missing Precambrian record of life. *Proc. Natl. Acad. Sci. USA* **2000**, *97*, 6947–6953. [CrossRef] [PubMed]
44. De Stefano, M.; Marino, D. Morphology and taxonomy of Amphicocconeisgen. nov. (Achnanthales, Bacillariophyceae, Bacillariophyta) with considerations on its relationship to other monoraphid diatom genera. *Eur. J. Phycol.* **2003**, *38*, 361–370. [CrossRef]
45. Pamirsky, I.E.; Golokhvast, K.S. Silaffins of Diatoms: From Applied Biotechnology to Biomedicine. *Mar. Drugs* **2013**, *11*, 3155–3167. [CrossRef]
46. Krishnamurti, D. The Raman spectra of aragonite, strontianite and witherite. *Proc. Indian Acad. Sci.—Sect. A* **1960**, *51*, 285–295. [CrossRef]
47. Görlich, S.; Samuel, A.J.; Best, R.J.; Seidel, R.; Vacelet, J.; Leonarski, F.K.; Tomizaki, T.; Rellinghaus, B.; Pohl, D.; Zlotnikov, I. Natural hybrid silica/protein superstructure at atomic resolution. *Proc. Natl. Acad. Sci. USA* **2020**, *117*, 31088–31093. [CrossRef]